

See discussions, stats, and author profiles for this publication at: <https://www.researchgate.net/publication/237093204>

Activation of C-H bond in methane by Pd atom from the bonding evolution theory perspective

ARTICLE *in* JOURNAL OF COMPUTATIONAL CHEMISTRY · AUGUST 2013

Impact Factor: 3.59 · DOI: 10.1002/jcc.23345 · Source: PubMed

CITATIONS

5

READS

34

1 AUTHOR:



[Anton S Nizovtsev](#)

Nikolaev Institute of Inorganic Chemistry SB ...

10 PUBLICATIONS 20 CITATIONS

SEE PROFILE

Activation of C–H Bond in Methane by Pd Atom from the Bonding Evolution Theory Perspective

Anton S. Nizovtsev

We report detailed study focused on the electron density redistribution during the simple oxidative addition reaction being the crucial stage of various catalytic processes. The bonding evolution theory based on the electron localization function and Thom's catastrophe theory shows that activation of methane's C–H bond by Pd atom consist of six elementary steps. The important feature revealed is the pronounced reorganization of Pd's outer core maxima corresponding to *N*-shell

electrons of metal. Electronic rearrangements identified in this model reaction are likely to be the case in the more complex reactions of the same type involving transition metal compounds and, in principle, can be observed by modern ultrafast spectroscopy and diffraction techniques. © 2013 Wiley Periodicals, Inc.

DOI: 10.1002/jcc.23345

Introduction

Activation of chemical bonds is a crucial step of various chemical processes, especially related to homogeneous catalysis, and has been intensively studied both experimentally and theoretically.^[1–14] Oxidative addition is an ubiquitous activation type including the insertion of metal into the bond; the reverse process is the reductive elimination. The coordination complexes of transition metals, in particular of Pd,^[5] are generally used as catalytically active species in these elementary reactions. Activation of small molecules, such as methane, is of considerable interest because it provides the possibility to convert the widespread but rather inert species into more useful products. It was experimentally established that only Rh,^[8] Ir,^[9] and Pt atoms^[10] are able to insert into methane's C–H bond in the gas phase, whereas interaction between Pd and CH₄ leads to formation of complex stable under external factors.^[11] However, owing to its closed-shell 4d¹⁰ electronic configuration, Pd atom can be considered as an attractive model system for Pd(0) complexes, namely their active center, being one of the most effective groups of catalysts for C–H activation.

In spite of substantial progress in studying of C–H activation, the most theoretical works concerning this problem are focused on the prediction of energy barriers and reaction energies, whereas the mechanism of oxidative addition in terms of electron density redistribution providing insight into features of the system's electronic structure is still unexplored. Bonding evolution theory (BET) is a powerful approach that allows one to monitor the changes in the electronic structure of reacting system.^[15] BET includes the topological analysis of electron localization function (ELF, $\eta(\mathbf{r})$)^[16–18] and Thom's catastrophe theory.^[19] Topological analysis of ELF gradient field^[20] provides a partition of molecular space into basins of attractors corresponding to chemically meaningful concepts such as atomic cores (core basins), bonds, and lone pairs (valence basins). Core basins, C(A) (A is the atomic symbol of the element), surround nuclei with atomic number $Z > 2$, valence

basins are represented by valence shell electrons of atoms in molecular systems and are labeled according to their synaptic order,^[21] that is, the number of core basins with which they share a common boundary. So, from the Lewis theory standpoint, V(A) monosynaptic basin stands for lone pair, V(A,X) disynaptic and V(A,X,Y) trisynaptic basins associate with two- and three-center bonds, respectively. By integrating electron density ($\rho(\mathbf{r})$) over the ELF basin volume (Ω), one can obtain the population of ELF basin by electrons (\bar{N}) being the quantitative characteristic of the method ($\bar{N}(\Omega_i) = \int_{\Omega_i} \rho(\mathbf{r}) d\mathbf{r}$). Thus, BET enables to determine the detailed electronic mechanism of the elementary act by constructing the sequence of simple chemical events (bond forming/breaking processes, creation/annihilation of lone pairs, etc.) followed by assignment of ELF topology changes on catastrophe theory. BET fundamentals are described in more detail elsewhere.^[15] A number of reaction types was investigated using BET including reactions of cycloaddition,^[22,23] cyclization,^[24] electron transfer,^[25] inversion substitution,^[26] and so forth. However, these were primarily organic reactions, whereas up to date, there are only few applications of BET to the reactions involving metal compounds^[27–32] that emphasizes the relevance of this work.

An important feature of BET is the ability to observe the flow of the electron density as the reaction proceeds, that is, BET gives access to the natural time scale of the chemical process. So, a recent study^[33] of the degenerate Cope rearrangement of semibullvalene showed good agreement between the results of time-dependent quantum simulations^[34] and those of BET.^[33] Thus, BET is capable to adequately predict the order, direction, and synchronicity of electron fluxes, providing rather valuable information when studying of reaction mechanisms at elementary level.

A. S. Nizovtsev

Nikolaev Institute of Inorganic Chemistry, Siberian Branch of the Russian Academy of Sciences, Academician Lavrentiev Avenue 3, Novosibirsk, 630090, Russian Federation

© 2013 Wiley Periodicals, Inc.

Here, we investigate activation of C—H bond in CH₄ by Pd atom from the BET perspective to establish electron density redistribution in the course of structural rearrangements.

Computational Details

To optimize geometric parameters, both all-electron scalar relativistic (ZORA-BLYP/TZ2P)^[35] and relativistic effective core potential (RECP)-based (B3LYP,^[36] M05,^[37] M06,^[38] CCSD^[39] with cc-pVTZ basis set for C and H atoms^[40] and cc-pVTZ-PP basis in conjunction with appropriate RECP for Pd, replacing 28 core electrons;^[41] for brevity, such combinations will be denoted as VnZ (*n* = T in this case), adding diffuse functions to basis sets will be designated by A-prefix) calculations were performed. ZORA-BLYP and B3LYP methods was chosen because they provide an energy of reaction under consideration close to that obtained from the high-level coupled cluster calculations.^[12–14] Moreover, B3LYP approach is traditionally used in the BET applications.^[22–33] We also tested a rather new M05 and M06 meta-hybrid functionals which were originally parametrized including transition metals and recommended for application in organo-metallic/inorganometallic chemistry.

Harmonic vibrational frequencies were treated analytically for all density functional theory (DFT) methods and by numerical differentiation of nuclear gradients for CCSD/VTZ one. Zero-point vibrational energies were computed from corresponding vibrational frequencies without scaling factors. The thermal correction to the enthalpy was calculated within rigid-rotor-harmonic-oscillator approximation and used for obtaining reaction enthalpies at 298 K.

The CCSD(T) coupled-cluster method^[42] was applied to CCSD/VTZ structures for calculating electron correlation. Energetic properties of the process being considered were calculated with the use of complete basis set (CBS) extrapolation technique by two-point extrapolation formula.^[43] Extrapolations were carried out for Hartree–Fock ($E_{HF,n} = E_{HF,CBS} + Ae^{-\alpha\sqrt{n}}$) and correlation energies ($E_{corr,n} = E_{corr,CBS} + \frac{B}{n^p}$) separately. Energy values calculated with (i) VTZ and VQZ ($\alpha = 5.46$, $\beta = 3.05$) and (ii) AVTZ and AVQZ ($\alpha = 5.79$, $\beta = 3.05$) basis sets were extrapolated to CBS limit ($n = 3, 4$).^[43] AVTZ/AVQZ extrapolation results were presented throughout the main text.

Stationary points were characterized by their harmonic vibrational frequencies as minima or saddle point [number of imaginary frequencies was equal to 0 and 1 for local minima and transition state (TS), respectively]. Minimum energy path was constructed at B3LYP/VTZ level in mass-weighted coordinates without symmetry constraints by using intrinsic reaction coordinate (IRC)^[44] algorithm with step size of 0.1 amu^{1/2}bohr.

All coupled-cluster computations were performed in the frozen core approximation. In ZORA-BLYP/TZ2P calculations, core potential was not used; the numerical integrals were evaluated with an accuracy of eight significant digits. Ultrafine grid was used in the all RECP-based DFT calculations.

ZORA-BLYP/TZ2P computations were performed with the use of ADF2010 program,^[45] whereas the remaining computations were carried out in Gaussian09 code.^[46] The natural population analysis (NPA) atomic charges^[47] were calculated as

implemented in Gaussian09. (Aug-)cc-pVnZ-PP basis sets were taken from the Environmental Molecular Sciences Laboratory (EMSL) database.^[48]

Topological calculations were performed with DGrid.^[49] Calculations in the framework of the atoms in molecules (AIM) theory^[20] were carried out for ZORA-BLYP/TZ2P densities only because of incorrect description of the electron density near the Pd arising at use RECP. B3LYP/VTZ densities were used for the ELF calculations in all points of the energy profile, whereas ZORA-BLYP/TZ2P ones were used for that in stationary points only. ELF basin populations were calculated for a rectangular parallelepipedic grid with a mesh size of 0.045 bohr. To increase the accuracy of basin integration, electron density grid was refined throughout with the precision of 0.1 e. Synapticity of the ELF basins was defined by an inspection of the corresponding zero-flux surfaces and was checked by an analysis of critical points (CPs) at ELF gradient field.

All species were considered in their ground states and in the gas phase. When calculating bond energies, spin-unrestricted formalism was applied to radicals. Comparison of the present results with the most accurate estimates from Refs. ^[12–14] is provided in Supporting Information.

Results and Discussion

Energy parameters of reaction

An energy diagram for reaction under study is shown in Figure 1. When interacting between Pd and CH₄, collisionally stabilized reactant complex (RC) is formed which is then converted into the reaction product (CH₃PdH), bypassing the TS. According to high-level CCSD(T)/CBS calculations, overall reaction is exothermic and proceeds without a barrier relative to reagents, whereas ZORA-BLYP/TZ2P and B3LYP/VTZ predict the presence of an energy barrier. The reason is the unsatisfactory description of dispersion interactions between Pd and two C—H bonds stabilizing RC by DFT methods leading to the overestimation of RC energy. The kinetic measurements suggest that the binding energy of the RC is at least 8 kcal/mol.^[6]

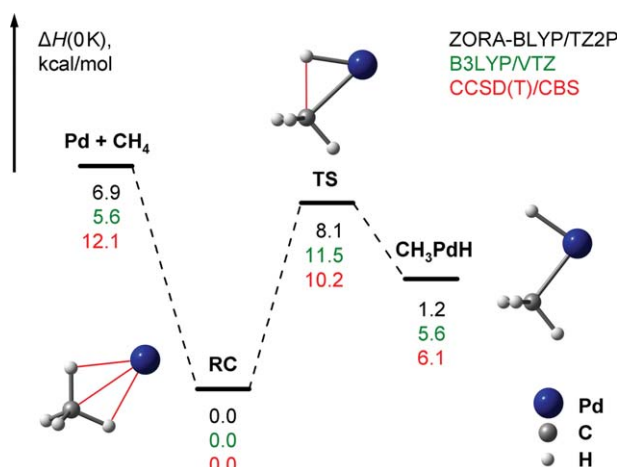


Figure 1. Schematic energy diagram for the C—H bond activation by Pd atom.

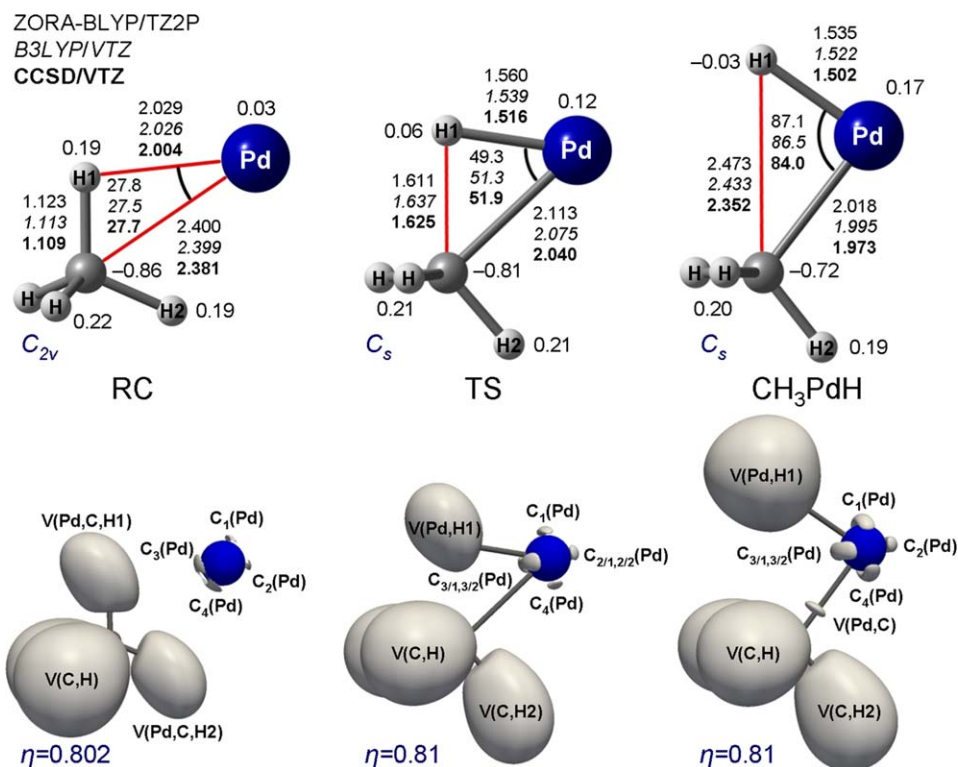


Figure 2. Atomic labeling, selected structural parameters (distances in Å, angles in degrees), and NPA charges (in |e|) computed at B3LYP/VTZ level (top) and ELF isosurfaces and attractors' labeling (bottom) for the stationary points considered. [Color figure can be viewed in the online issue, which is available at wileyonlinelibrary.com.]

Indeed, CCSD(T)/CBS gives a value equal to 12.1 kcal/mol, whereas ZORA-BLYP/TZ2P and B3LYP/VTZ underestimate the RC binding energy by 5.2 kcal/mol and 6.5 kcal/mol, respectively. However, the key point for us is the accuracy of the central barrier height, that is, energy of TS relative to that of RC. Therefore, error in the RC binding energy plays a minor role.

As one can see from Figures 1 and 2, B3LYP/VTZ results are comparable with CCSD(T)/CBS ones in energy (errors in ΔH_0° for barrier height and energy of the reaction are 1.3 kcal/mol and -0.5 kcal/mol, respectively), which is in line with preceding benchmarks,^[12–14] and with CCSD/VTZ ones in geometrical parameters (the difference in the interatomic distances is less than 0.035 Å excepting $r(\text{C}-\text{H1})$ in CH₃PdH). ZORA-BLYP/TZ2P predictions have a lower but, in general, acceptable accuracy. Surprisingly, the worst results among the DFT methods used exhibit the meta-hybrid functionals, M05 and M06, specially designed for the calculation of transition metal compounds (see Supporting Information). They substantially overestimate the energy of both TS (>7 kcal/mol) and CH₃PdH (>10 kcal/mol) relative to RC that makes them unsuitable for further using in this work.

Thus, we used B3LYP/VTZ approximation to construct the energy profile along the reaction coordinate as well as to extract the electron density for the ELF topological calculations. For comparison, ELF analysis in stationary points was performed for the electron densities obtained by all-electron ZORA-BLYP/TZ2P method.

Bonding analysis of stationary points

ELF isosurfaces and basins' labeling for the stationary points on the reaction path are presented in Figure 2. It is clearly seen that all species have ELF attractors surrounding Pd core. Their number is equal to 4, 6, and 5 for RC, TS, and CH₃PdH, respectively. They represent outer core maxima (OCM)^[50] of Pd arising on the interaction of its *N*-shell electrons with the electrons of neighboring atoms, OCM being located around the atomic nucleus of the metal so as to minimize Pauli repulsion. It should be noted that the OCM are analogous to charge concentrations (CCs) revealed by Gillespie et al.,^[51] but they are different in the scalar field considered: OCM are defined at ELF field, CCs are associated with Laplacian of the electron density ($L(\mathbf{r}) = -\nabla^2 \rho(\mathbf{r})$). The number and arrangement of the OCM and CCs are identical as it has been previously found for the transition metal compounds.^[52] Furthermore, the existence of CCs was experimentally confirmed using precise diffraction methods.^[53] A similar structuring of ELF in the outer core regions was observed for other palladium compounds: [PdCl₄]²⁻, [PdCl₃(H₂O)]⁻, and [PdCl₂(H₂O)₂],^[54] as well as for [Pd(Ph)(NH₂)(PH₃)] and [Pd(Ph)(NⁱBu₂)(PH₃)].^[55] However, in the latter case, ELF core basins were assigned to the lone pairs of Pd.

Pd atom in its ¹S₀ ground state possesses an unique [Kr]4d¹⁰5s⁰ electron configuration, that is, it has no electrons in the valence shell ($n = 5$). Hence, the atom in the molecular system should have only core basins of ELF. Table 1 shows that the state of Pd core may be assigned to [Kr]4d¹⁰5s⁰ and

Table 1. Reaction coordinates (IRC, amu^{1/2}bohr), relevant structural parameters (r in Å, α in degrees), ELF basin populations^[a] (\bar{N} , e) and charge transfer from Pd^[b] (CT, e) for the initial and final points of SSDs defined on the IRC path. ΔE (kcal/mol) is energy difference between extreme points within each SSD.

SSD	I	II	III	IV	V	VI							
IRC	RC	−3.1	−3.0	−2.0	−1.9	−1.3	−1.2	−0.4	−0.3	TS	0.8	0.9	CH ₃ PdH
<i>r</i> (Pd—C)	2.399	2.367	2.353	2.220	2.207	2.140	2.130	2.084	2.081	2.075	2.053	2.050	1.995
<i>r</i> (Pd—H1)	2.026	1.997	1.982	1.800	1.781	1.677	1.662	1.565	1.557	1.539	1.519	1.519	1.522
<i>r</i> (Pd—H2)	2.026	2.008	2.004	2.036	2.049	2.155	2.177	2.322	2.335	2.371	2.458	2.468	2.483
<i>r</i> (C—H1)	1.113	1.115	1.116	1.140	1.143	1.177	1.186	1.450	1.496	1.637	2.005	2.049	2.433
α(C—Pd—H1)	27.5	28.0	28.2	30.7	31.0	33.2	33.7	44.0	45.8	51.3	66.3	68.2	86.5
C(C)	2.10 (2.11)	2.10	2.09	2.10	2.10	2.10	2.10	2.09	2.09	2.09 (2.10)	2.09	2.09	2.09 (2.10)
C ₁ (Pd)	4.57 (4.34)	4.45	4.44	3.74	3.63	3.26	3.26	3.44	3.50	3.64 (3.62)	3.91	3.93	4.19 (4.17)
C ₂ (Pd)	4.57 (4.73)	4.64										4.24	3.97 (4.13)
C _{2/1} (Pd)			2.09	2.58	2.64	2.77	2.68	2.48	2.47	2.37 (2.46)	2.18		
C _{2/2} (Pd)			2.55	2.55	2.55	2.68	2.75	2.48	2.40	2.28 (2.38)	2.09		
C ₃ (Pd)	4.36 (4.42)	4.50	4.55	5.19									
C _{3/1} (Pd)					2.43	2.95	2.98	2.92	2.88	2.76 (2.60)	2.54	2.51	2.01 (2.21)
C _{3/2} (Pd)					2.79	2.86	2.89	2.83	2.79	2.67 (2.69)	2.45	2.43	2.59 (2.29)
C ₄ (Pd)	4.42 (4.37)	4.32	4.27	3.79	3.80	3.25	3.18	3.31	3.39	3.60 (3.58)	3.93	3.96	4.18 (4.19)
V(Pd,C)									0.88	0.95 (0.89)	1.02	1.03	1.09 (1.04)
V(Pd,H1)									1.45	1.47 (1.44)	1.58	1.59	1.67 (1.67)
V(Pd,C,H1)	1.99 (2.00)	2.00	2.00	2.02	2.02	2.08	2.10	2.30					
V(Pd,C,H2)	2.00 (2.00)	1.99	1.99	2.03	2.03	2.06							
V(C,H2)							2.06	2.04	2.04	2.04 (2.04)	2.04	2.04	2.05 (2.05)
V(C,H)	1.99 (1.99)	1.99	1.99	1.99	2.00	1.99	1.99	2.04	2.05	2.06 (2.06)	2.07	2.07	2.06 (2.07)
CT	0.08 (0.14)	0.09	0.10	0.15	0.16	0.23	0.26	0.54	0.57	0.68 (0.67)	0.90	0.93	1.06 (1.01)
ΔE		0.0		1.6		3.0		7.0		0.8 ^[c]	−2.3		−2.9
[a] ELF basin populations computed with ZORA-BLYP/TZ2P densities are given in parentheses. For that, ZORA-BLYP/TZ2P optimize structures were used.													
[b] CT=18−∑ _i <i>N</i> [C _i (Pd)]. [c] Energy difference between first point of SSD V and TS.													

[a] ELF basin populations computed with ZORA-BLYP/TZ2P densities are given in parentheses. For that, ZORA-BLYP/TZ2P optimize structures were used.

[b] CT = $18 - \sum_i \bar{N}[C_i(\text{Pd})]$. [c] Energy difference between first point of SSD V and TS.

[Kr]4d⁹5s⁰ configuration in RC and CH₃PdH, respectively, that is, the transfer of about one electron accompanied by the formation of chemical bonds has happened in the course of reaction. It is important to stress that this result is valid for the electron density obtained from both RECP and all-electron calculations. It allows us to use B3LYP/VTZ electron density in further topological calculations. Changes in the NPA charges (Fig. 2) also indicate a gradual electron density transfer from Pd. How to explain the formation of bonds with Pd participation in terms of the ELF if Pd does not have the valence electrons required? The answer to this question can be obtained by considering the electronic state of Pd atom as a superposition of [Kr]4d¹⁰5s⁰ and [Kr]4d⁹5s¹ states. It is worth to note that the latter is related to the ground state configuration of Pt ([Xe]4f¹⁴5d⁹6s¹), a heavier analog of Pd activating a methane at room temperature.^[10] Thus, within the reaction, the electron density is transferred to the valence region, enabling the electrons of metal contribute to the ELF valence basins. This approach has been applied to the interpretation of metal-ligand bonds in transition metal compounds, particularly, to determining of electronic configurations of the metal's cores.^[52] In addition, it enabled to account for the discrepancies in the bonding patterns on interaction of Pd atom with different adsorption centers.^[56]

At RC, interaction of two C—H bonds with Pd leads to the formation of ELF basins, which should be formally classified as protonated trisynaptic basins, V(Pd,C,H_n), reflecting three-center two-electron bonds between the atoms because V(C,H1) and V(C,H2) attractors are connected with C₃(Pd) and C₄(Pd) ones, respectively, by means of (3,−1) CPs. However, as seen from the

NPA charges (Fig. 2), electron density in RC is hardly transferred from the Pd atom, so these electrons are almost completely concentrated in the C—H bonds. Small contribution of Pd electrons into V(Pd,C,H_n) basins ($\bar{N}[\text{V}(\text{Pd},\text{C},\text{H}_n)|\text{Pd}] = 0.05$ e), as calculated from the ELF/AIM intersection procedure,^[57] suggests the same.

CH₃PdH molecule has unusual bonds. Population of V(Pd,H1) basin is about 1.7 e, which may correspond both to the covalent Pd—H1 bond and, owing to position of ELF basin typical for bonds involving hydrogen, to the ionic one with the electrons centered on H1. In the latter case, H1 will be a hydride ion. However, NPA atomic charges (Fig. 2) display rather weak polarization of Pd—H1 bond, as expected from the small difference in electronegativities of the elements. Moreover, the results of AIM calculations ($\rho(\mathbf{r}_b) = 1.066$ e·Å^{−3}, $\nabla^2\rho(\mathbf{r}_b) = -0.193$ e·Å^{−5}, $|V(\mathbf{r}_b)|/G(\mathbf{r}_b) = 2.021$, $H(\mathbf{r}_b) = -0.695$ Hartree·Å^{−3}) indicate the *shared*-type interaction between these two atoms. Thus, the case of covalent bonding is more likely.

A more complex case is the Pd—C bond. As shown in Figure 2, the appropriate ELF basin is displaced to C atom and is carried around 1 e. It is important, that this basin is immediately formed after the C—H1 bond breaking. So, the CH₃ and PdH moieties may be biradically coupled from the ELF standpoint. To verify the assumption, we performed ELF calculations for CH₃ and PdH radicals taken in their CH₃PdH geometries. The populations of ELF basins turned out to almost coincide ($\bar{N}[\text{V}(\text{C})]/\bar{N}[\text{V}(\text{Pd},\text{C})]$: 0.95 e (CH₃) vs. 1.09 e (CH₃PdH); $\bar{N}[\text{V}(\text{Pd},\text{H1})]$: 1.64 e (PdH) vs. 1.67 e (CH₃PdH)). However, intersection of V(Pd,C) basin with AIM ones^[57] corresponding to Pd and C atoms yields the contribution of 0.32 e from Pd and

0.77 e from C that does not support initial assumption. Also, B3LYP/VTZ wavefunction of CH_3PdH proved to be stable under perturbations within the standard *stable=opt* procedure, indicating the closed-shell character of the wavefunction and thus the absence of biradical nature in the ground state of CH_3PdH . Indeed, AIM parameters ($\rho(\mathbf{r}_b) = 0.857 \text{ e} \cdot \text{\AA}^{-3}$, $\nabla^2\rho(\mathbf{r}_b) = 2.217 \text{ e} \cdot \text{\AA}^{-5}$, $|V(\mathbf{r}_b)|/G(\mathbf{r}_b) = 1.700$, $H(\mathbf{r}_b) = -0.364 \text{ Hartree} \cdot \text{\AA}^{-3}$) denote *intermediate*-type interaction between Pd and C atoms implying some degree of covalence, but less compared to Pd—H1 bond where Pd contribution into the $V(\text{Pd},\text{H1})$ basin is 0.61 e. At the same time, *closed-shell*-type, that is, ionic in this case, interaction between atoms in the Pd—C bond takes place as well. So, one can conclude that Pd—C bond has a dual covalent/ionic nature.

It has been previously reported^[58] that the M—C interactions in MCH_3 ($\text{M} = \text{K—Mn}$) have predominantly ionic nature. They possess of AIM parameters close to Pd—C ones, but populations of their $V(\text{M},\text{C})$ basins are significantly higher, 1.6–1.9 e. Interestingly, ELF topology of CH_3 fragment corresponds to CH_3^- anion rather than CH_3^\cdot radical as in the case of CH_3PdH . The same conclusion about the ionicity of M—C bond was also drawn by Solà and coworkers for MCH_3 ($\text{M} = \text{Li, Na, K}$) compounds.^[59]

In addition, Pd—H bond is stronger than Pd—C one (ΔH_{298}° values for the $\text{CH}_3\text{PdH} \rightarrow \text{CH}_3\text{Pd} + \text{H}$ and $\text{CH}_3\text{PdH} \rightarrow \text{CH}_3 + \text{PdH}$ processes are equal to 65.0 kcal/mol and 54.7 kcal/mol, respectively, at the CCSD(T)/CBS level).

Catastrophes along reaction coordinate

From the BET standpoint, the path of elementary chemical reaction is viewed as a sequence of structural stability domains (SSDs) within which all the CPs are hyperbolic. The transition between two consecutive SSDs is fulfilled by using catastrophe that occurs at the bifurcation point where at least one CP is nonhyperbolic. The catastrophes are identified according to Thom's classification. Each SSD includes points of the reaction path with the same number of CPs of each type in the ELF gradient field. Depending on the level of detail, BET can be applied in different variants. Here, we use BET at the *current* level, in which only the evolution of ELF basins is analyzed, with additional consideration of the molecular graph built from the ELF gradient field CPs to ascertain when synaptic order of the $V(\text{Pd},\text{C},\text{H}_2)$ basin is changed.

Reaction energy profile is depicted in Figure 3. Carrying out ELF topological calculations in the points of profile, the presence of six SSDs, and, consequently, five bifurcation points was revealed. The events underlying transitions between SSDs are presented in Figure 4; ELF basin populations are summarized in Table 1.

ELF topology of the system is rapidly changed after the beginning of reaction, thus forming the shortest domain, SSD I, ranging from RC to $\text{IRC} = -3.1 \text{ amu}^{1/2}\text{bohr}$. Within SSD I, structural parameters are slightly varied (interatomic distances are no more than 0.03 Å, $\alpha(\text{C—Pd—H1})$ is increased by 0.5°), and energy of the system remains constant. At RC, each of $\text{C}_1(\text{Pd})$ — $\text{C}_4(\text{Pd})$ basins is populated by about of 4.5 electrons, constituting the

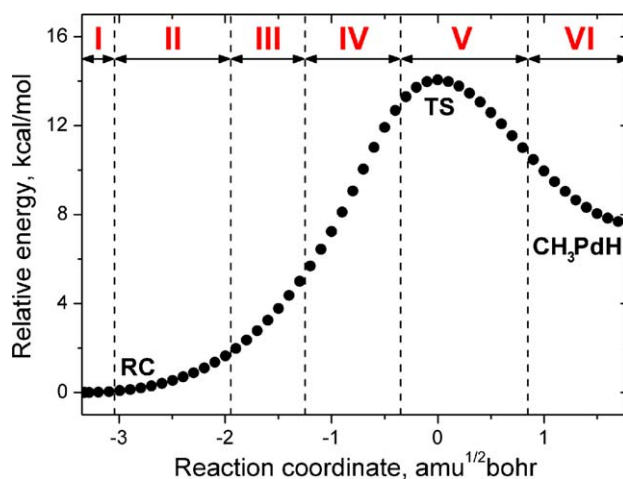


Figure 3. Energy profile for the C—H bond activation by Pd atom calculated at B3LYP/VTZ level. Bifurcation points along reaction coordinate are shown by dashed lines. [Color figure can be viewed in the online issue, which is available at wileyonlinelibrary.com.]

Pd's *N*-shell, which are then undergone a minor redistribution: for $\text{C}_2(\text{Pd})$ and $\text{C}_3(\text{Pd})$ basins an increase of the population by 0.07 e and 0.14 e is observed, whereas $\bar{N}[\text{C}_1(\text{Pd})]$ and $\bar{N}[\text{C}_4(\text{Pd})]$, on the contrary, is decreased by 0.12 e and 0.10 e, respectively.

SSD II begins at $-3.0 \text{ amu}^{1/2}\text{bohr}$ from the separation of $\text{C}_2(\text{Pd})$ basin into two parts, $\text{C}_{2/1}(\text{Pd})$ with $\bar{N}=2.09$ e and $\text{C}_{2/2}(\text{Pd})$ with $\bar{N}=2.55$ e (Fig. 4a). Together with that, transformation of the CP of index 0 ($\text{C}_2(\text{Pd})$) into two analogous ones ($\text{C}_{2/1}(\text{Pd})$ and $\text{C}_{2/2}(\text{Pd})$) and bond CP (i.e., CP of index 1) between them takes place. Thus, the catastrophe can be classified as a cusp-type. Then, the approaching of Pd with H1 and C by 0.182 and 0.133 Å, respectively, accompanied by a total energy increase in 1.6 kcal/mol causes pronounced outflow of electron density from the axial $\text{C}_1(\text{Pd})$ and $\text{C}_4(\text{Pd})$ basins to equatorial $\text{C}_{2/1}(\text{Pd})$, $\text{C}_{2/2}(\text{Pd})$ and $\text{C}_3(\text{Pd})$ ones. It leads to equalization of the populations in these two groups of basins: $\text{C}_1(\text{Pd})$ and $\text{C}_4(\text{Pd})$ are filled by 3.74 e and 3.79 e, respectively; $\bar{N}[\text{C}_3(\text{Pd})]$ is the sum of $\bar{N}[\text{C}_{2/1}(\text{Pd})]$ and $\bar{N}[\text{C}_{2/2}(\text{Pd})]$, 5.19 e vs. 5.13 e.

SSD III is characterized by increasing of the number of metal's OCM. Separation of $\text{C}_3(\text{Pd})$ ($\bar{N}=5.19$ e) basin gives rise $\text{C}_{3/1}(\text{Pd})$ and $\text{C}_{3/2}(\text{Pd})$ ones at $-1.9 \text{ amu}^{1/2}\text{bohr}$ populated by 2.43 e and 2.79 e, respectively (Fig. 4b). This catastrophe is similar to the previous one and likewise belongs to the cusp-type. Within SSD III, electrons of Pd continue to be concentrated in the regions of equatorial core basins, but non-equivalence of near ($\text{C}_{3/1}(\text{Pd})$ and $\text{C}_{3/2}(\text{Pd})$) and far ($\text{C}_{2/1}(\text{Pd})$ and $\text{C}_{2/2}(\text{Pd})$) ones with respect to ligands becomes noticeable. At $\text{IRC} = -1.3 \text{ amu}^{1/2}\text{bohr}$, the first group holds by 0.36 e more than the second one. At the same time, a populations of $\text{C}_1(\text{Pd})$ and $\text{C}_4(\text{Pd})$ basins are significantly decreased, reaching the about 3.3 e values in the last point of the domain.

The most energy increment is fallen at the SSD III ($\Delta E = 3.0$ kcal/mol) and SSD IV ($\Delta E = 7.0$ kcal/mol). The reason is the weakening of C—H1 bond caused by its stretching by 0.307 Å that is not fully compensated by forming of Pd—C and Pd—H1 bonds. It is interesting that at these stages the population of $V(\text{Pd},\text{C},\text{H1})$ basin responsible for three-center interaction

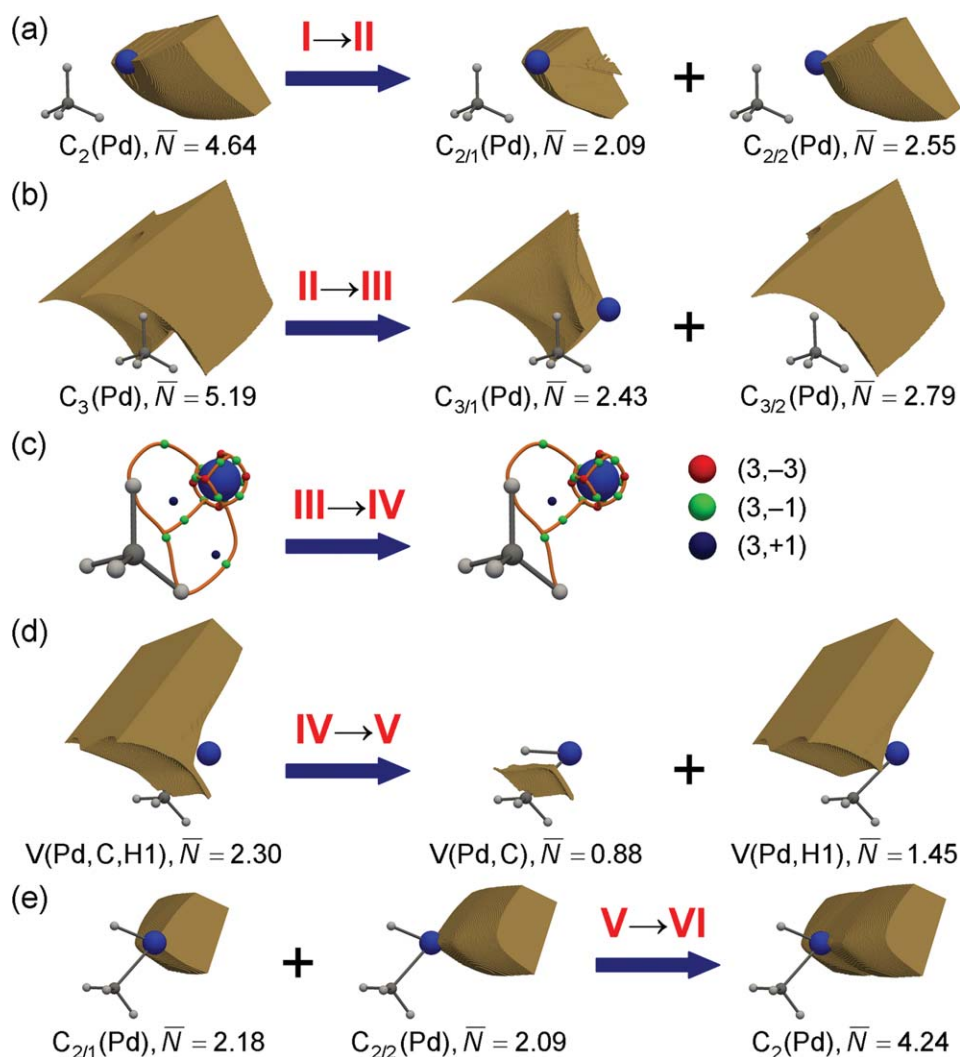


Figure 4. Changes in ELF topology responsible for transitions between SSDs within the C–H bond activation by Pd atom. The relevant ELF basins and their populations (in e) are given in (a), (b), (d), and (e). Molecular graphs constructed from the ELF gradient field critical points [(c), partly shown; paths between (3, -3) and (3, -1) critical points are depicted by gold lines] display a conversion of $V(\text{Pd}, \text{C}, \text{H2})$ attractor into $V(\text{C}, \text{H2})$ one (positions of these attractors almost coincide with that of H2 atom).

between the atoms significantly increases ($\Delta\bar{N}=0.28$ e). It denotes the rising contribution of Pd to the bonding and correlates with changing of the charge transfer (CT) parameter.

Along SSD IV, the number of attractors remains the same; however, the analysis of the CPs in the ELF gradient field specially performed revealed a change of the basin's synaptic order. So, $V(\text{Pd}, \text{C}, \text{H2})$ trisynaptic basin becomes $V(\text{C}, \text{H2})$ disynaptic one (Fig. 4c). At this transition, two CPs of different parity disappear, that of index 1 [(3, -1) CP, joining $V(\text{Pd}, \text{C}, \text{H2})$ and $C_4(\text{Pd})$ attractors] and 2 [(3, +1) CP between Pd, C and H2], to give a wandering (noncritical) point that implies the fold-type catastrophe. From the quantum chemical topology (QCT) viewpoint, it is in line with the conversion of three-center interaction to two-center one.

The transition from SSD IV to SSD V is a crucial step of the reaction, because at this stage the system of chemical bonds is changed. Population of the $V(\text{Pd}, \text{C}, \text{H1})$ basin reaches its limit (2.30 e) at $-0.4 \text{ amu}^{1/2}\text{bohr}$, whereupon it is divided into two parts, $V(\text{Pd}, \text{C})$ and $V(\text{Pd}, \text{H1})$, associating with Pd–C and Pd–H1

bonds, respectively (Fig. 4d). The catastrophe joining these two domains belongs to a cusp-type, as evidenced by the occurrence of the two attractors, $V(\text{Pd}, \text{C})$ and $V(\text{Pd}, \text{H1})$, and (3, -1) CP between them from the $V(\text{Pd}, \text{C}, \text{H1})$ attractor. This elementary chemical event takes place in the vicinity of TS and corresponds to the C–H1 bond breaking from the QCT standpoint.

Starting from SSD IV to the end of the reaction, axial core basins are gradually populated by electrons at the expense of four equatorial ones, distinctions between which become clearer. So, if at the beginning of SSD IV, total population of $C_{3/1}(\text{Pd})$ and $C_{3/2}(\text{Pd})$ basins exceeds that of $C_{2/1}(\text{Pd})$ and $C_{2/2}(\text{Pd})$ ones by 0.44 e, at domain's last point the difference is 0.79 e. In SSD V, nonequivalence persists, reaching its maximum at $-0.3 \text{ amu}^{1/2}\text{bohr}$ (0.80 e), and then slowly decreases to 0.72 e at the point corresponding $\text{IRC} = 0.8 \text{ amu}^{1/2}\text{bohr}$. At the same time, $\bar{N}[C_1(\text{Pd})]$ and $\bar{N}[C_4(\text{Pd})]$ become equal to about 3.9 e. In the longest SSD V which includes TS, both the Pd–C and Pd–H1 bond lengths and the populations of

corresponding valence basins are approached to their equilibrium values. It is accompanied by a CT from Pd ($\Delta\text{CT} = 0.33\text{ e}$) and a total energy lowering in 2.3 kcal/mol.

Subsequently, $\text{C}_{2/1}(\text{Pd})$ ($\bar{N}=2.18\text{ e}$) and $\text{C}_{2/2}(\text{Pd})$ ($\bar{N}=2.09\text{ e}$) basins are back combined into $\text{C}_2(\text{Pd})$ ($\bar{N}=4.24\text{ e}$) one in a cusp catastrophe, thus forming the final domain, SSD VI (Fig. 4e). During SSD VI, $\alpha(\text{C}-\text{Pd}-\text{H}1)$ bond angle is experienced a major variation (from 68.2° to 86.5°) leading to increase of distance between Pd and H2 by $\sim 0.4\text{ \AA}$. In the subsystem of OCM basins, electron density is continued to flow toward the axial basins ($\Delta\bar{N}=0.48\text{ e}$) by reducing the total population of the equatorial ones ($\Delta\bar{N}=-0.61\text{ e}$), a part of the charge ($\Delta\text{CT} = 0.13\text{ e}$) being donated to the ligands. As a result, basin population of $\text{C}_1(\text{Pd})$ and $\text{C}_4(\text{Pd})$ comes to about 4.2 e, $\text{C}_2(\text{Pd})$ is filled with 3.97 e, and the sum of $\bar{N}[\text{C}_{3/1}(\text{Pd})]$ and $\bar{N}[\text{C}_{3/2}(\text{Pd})]$ becomes equal to 4.60 e. All of this stabilizes the system by 2.9 kcal/mol.

Thus, activation of methane's C—H bond by Pd atom can be represented as a $6-[\text{C}^\dagger][\text{C}^\dagger][\text{F}][\text{C}^\dagger][\text{C}]-0$ according to the BET nomenclature.^[22] That is the reaction includes six steps or SSDs, separated by five bifurcation points with a cusp-cusp-fold-cusp-cusp sequence of catastrophes, three of which being characterized by an increase of the number of basins (indicated by \dagger symbol), whereas in remaining cases a decrease of synaptic order ($[\text{F}]$) and that of the number of basins ($[\text{C}]$) occurs; bold symbol ($[\text{C}^\dagger]$) denotes a bond formation. Because the reaction proceeds with the increasing of the number of basins ($\Delta\mu > 0$), one can conclude that it is polymorphic.^[15]

As it follows from the comparison of electron density distribution around Pd atom in RC and CH_3PdH , electron from the metal is mainly transferred at the cost of depopulation of $\text{C}_2(\text{Pd})$ basin ($\Delta\bar{N} = -0.60\text{ e}$) and, to a less extent, $\text{C}_1(\text{Pd})$ and $\text{C}_4(\text{Pd})$ axial basins. This happens in a rather subtle way involving all ELF core basins of Pd which means considerable reorganization of its *N*-shell electrons. It is also worth noting the smaller electron density transfer from Pd to $\text{V}(\text{C},\text{H})$ and $\text{V}(\text{C},\text{H}2)$ basins ($\sim 0.2\text{ e}$) as compared with that of to $\text{V}(\text{Pd},\text{H}1)$ and $\text{V}(\text{Pd},\text{C})$ ones. In addition, a merging of the Pd core basins coincides with the total energy lowering, while their separation correlates with the opposite energy effect.

Evolution of Pd's OCM

What is the reason of multiple transformations (see Fig. 5) in the Pd's core basins? As mentioned above, while interacting with ligands' electrons, the *N*-shell of Pd loses its spherical symmetry to minimize Pauli repulsion. As a result, the electrons with the opposite spins are localized giving OCM which

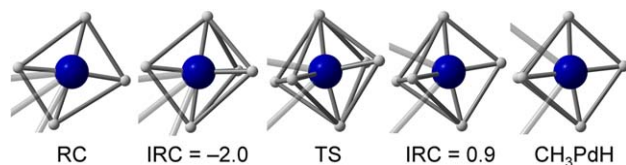


Figure 5. Evolution of Pd's OCM during the C—H bond activation. Reaction coordinates (IRC) are given in $\text{amu}^{1/2}\text{bohr}$. [Color figure can be viewed in the online issue, which is available at wileyonlinelibrary.com.]

affect the relative position of the H and CH_3 ligands were found to interact with the metal's core sufficiently strong.^[52] So, the OCM arrangement enables to explain the structure of molecular systems being the physical basis of the valence-shell electron pair repulsion model. In fact, CH_3PdH has a bent structure as predicted by Gillespie et al. for these ligands.^[52] To the best of our knowledge, the evolution of transition metal's OCM in a chemical reaction has not been considered in detail, although such studies were found to provide deep insight into processes underlying phase transitions in crystals.^[50]

Pd atom in RC has four OCM that are ordered around the metal as a rhombus. In SSD II, the fifth OCM appears from the side opposite to the ligands, giving attractors to form a trigonal bipyramid. The appearance of the sixth OCM in SSD III leads to the formation of octahedron corresponding to the most stable OCM arrangement in the whole process which is retained to the end of SSD V. A merging of $\text{C}_{2/1}(\text{Pd})$ and $\text{C}_{2/2}(\text{Pd})$ basins in SSD VI gives rise a trigonal bipyramid again, but the ordering of its base's vertices is different from the previous one. After that, the subset of $\text{C}_1(\text{Pd})$ – $\text{C}_4(\text{Pd})$ basins is no longer changed. In all cases, the ligands are positioned so as to minimize electrostatic repulsion between electrons populating their ELF basins and electrons from the OCM ones.^[60] As the reaction proceeds, the ligands are originally occupied sites opposite edges (SSDs I–II) and afterwards they stand opposite the faces (SSDs III–VI) of geometric figures formed by OCM of Pd. It seems to be due to the increase of interaction between electronic subsystems of approaching species.

On the basis of the data obtained, one can expect the resembling electronic structure changes during the more complex reactions of the same type. Though Pd was regarded as a metal, we suspect that OCM of other transition metals also will be undergone by substantial reorganization along insertion into the bond.

Conclusions


In summary, we shed some light on the electron density redistribution in the course of C—H bond activation in CH_4 by Pd atom being a simple model for oxidative addition. From the BET perspective, the reaction includes six steps connected by five bifurcation points with the $[\text{C}^\dagger][\text{C}^\dagger][\text{F}][\text{C}^\dagger][\text{C}]$ consequence of catastrophes, four of which corresponds to the subtle changes in the system of Pd's ELF core basins. We believe that our work will be useful when studying chemical reactions with the participation of transition metal compounds by advanced experimental techniques enabling to observe electron motion,^[61,62] and will promote deeper understanding of catalytic processes' mechanisms.

Acknowledgment

A. S. N. is grateful to Prof. S. G. Kozlova, Dr. M. R. Ryzhikov, and Dr. I. V. Mirzaeva for valuable discussions and to Prof. A. Savin for helpful comments.

Keywords: bond activation • reaction mechanism • electronic structure • electron localization function • catastrophe theory

How to cite this article: A. S. Nizovtsev, *J. Comput. Chem.* **2013**, *34*, 1917–1924. DOI: 10.1002/jcc.23345

 Additional Supporting Information may be found in the online version of this article.

- [1] R. H. Crabtree, *Chem. Rev.* **1995**, *95*, 987.
- [2] B. A. Arndtsen, R. G. Bergman, T. A. Mobley, T. H. Peterson, *Acc. Chem. Res.* **1995**, *28*, 154.
- [3] A. E. Shilov, G. B. Shul'pin, *Chem. Rev.* **1997**, *97*, 2879.
- [4] D. Balcells, E. Clot, O. Eisenstein, *Chem. Rev.* **2010**, *110*, 749.
- [5] J. Tsuji, *Palladium Reagents and Catalysis: Innovations in Organic Synthesis*; Wiley: Chichester, **1995**.
- [6] J. J. Carroll, J. C. Weisshaar, *J. Am. Chem. Soc.* **1993**, *115*, 800.
- [7] J. J. Carroll, K. L. Haug, J. C. Weisshaar, M. R. A. Blomberg, P. E. M. Siegbahn, M. Svensson, *J. Phys. Chem.* **1995**, *99*, 13955.
- [8] M. L. Campbell, *J. Am. Chem. Soc.* **1997**, *119*, 5984.
- [9] M. L. Campbell, *J. Phys. Chem. A* **1997**, *101*, 9377.
- [10] M. L. Campbell, *J. Chem. Soc., Faraday Trans.* **1998**, *94*, 353.
- [11] M. L. Campbell, *Chem. Phys. Lett.* **2002**, *365*, 361.
- [12] G. T. de Jong, M. Solà, L. Visscher, F. M. Bickelhaupt, *J. Chem. Phys.* **2004**, *121*, 9982.
- [13] G. T. de Jong, D. P. Geerke, A. Diefenbach, F. M. Bickelhaupt, *Chem. Phys.* **2005**, *313*, 261.
- [14] M. M. Quintal, A. Karton, M. A. Iron, A. D. Boese, J. M. L. Martin, *J. Phys. Chem. A* **2005**, *110*, 709.
- [15] X. Krokidis, S. Noury, B. Silvi, *J. Phys. Chem. A* **1997**, *101*, 7277.
- [16] A. D. Becke, K. E. Edgecombe, *J. Chem. Phys.* **1990**, *92*, 5397.
- [17] B. Silvi, A. Savin, *Nature* **1994**, *371*, 683.
- [18] A. Savin, R. Nesper, S. Wengert, T. F. Fässler, *Angew. Chem. Int. Ed.* **1997**, *36*, 1808.
- [19] R. Thom, *Structural Stability and Morphogenesis: An Outline of a General Theory of Models*; W. A. Benjamin, Inc.: Reading, MA, **1975**.
- [20] R. F. W. Bader, *Atoms in Molecules: A Quantum Theory*; Clarendon Press: Oxford, UK, **1990**.
- [21] B. Silvi, *J. Mol. Struct.* **2002**, *614*, 3.
- [22] S. Berski, J. Andrés, B. Silvi, L. R. Domingo, *J. Phys. Chem. A* **2006**, *110*, 13939.
- [23] (a) V. Polo, J. Andrés, S. Berski, L. R. Domingo, B. Silvi, *J. Phys. Chem. A* **2008**, *112*, 7128; (b) P. González-Navarrete, L. R. Domingo, J. Andrés, S. Berski, B. Silvi, *J. Comput. Chem.* **2012**, *33*, 2400.
- [24] (a) J. Andrés, S. Berski, L. R. Domingo, V. Polo, B. Silvi, *Curr. Org. Chem.* **2011**, *15*, 3566; (b) J. Andrés, S. Berski, L. R. Domingo, P. González-Navarrete, *J. Comput. Chem.* **2012**, *33*, 748.
- [25] J. Kalinowski, S. Berski, A. J. Gordon, *J. Phys. Chem. A* **2011**, *115*, 13513.
- [26] V. Polo, P. González-Navarrete, B. Silvi, J. Andrés, *Theor. Chem. Acc.* **2008**, *120*, 341.
- [27] S. Chiodo, O. Kondakova, M. C. Michellini, N. Russo, E. Sicilia, *Inorg. Chem.* **2003**, *42*, 8773.
- [28] M. C. Michellini, E. Sicilia, N. Russo, M. E. Alikhani, B. Silvi, *J. Phys. Chem. A* **2003**, *107*, 4862.
- [29] S. Chiodo, O. Kondakova, M. C. Michellini, N. Russo, E. Sicilia, A. Irigoras, J. M. Ugalde, *J. Phys. Chem. A* **2004**, *108*, 1069.
- [30] M. E. Alikhani, M. C. Michellini, N. Russo, B. Silvi, *J. Phys. Chem. A* **2008**, *112*, 12966.
- [31] S. Berski, F. R. Sensato, V. Polo, J. Andrés, V. S. Safont, *J. Phys. Chem. A* **2011**, *115*, 514.
- [32] A. S. Nizovtsev, S. G. Kozlova, *J. Phys. Chem. A* **2013**, *117*, 481.
- [33] P. González-Navarrete, J. Andrés, S. Berski, *J. Phys. Chem. Lett.* **2012**, *3*, 2500.
- [34] D. Andrae, I. Barth, T. Bredtmann, H. -C. Hege, J. Manz, F. Marquardt, B. Paulus, *J. Phys. Chem. B* **2011**, *115*, 5476.
- [35] (a) E. van Lenthe, E. J. Baerends, J. G. Snijders, *J. Chem. Phys.* **1993**, *99*, 4597; (b) E. van Lenthe, E. J. Baerends, J. G. Snijders, *J. Chem. Phys.* **1994**, *101*, 9783; (c) E. van Lenthe, R. van Leeuwen, E. J. Baerends, J. G. Snijders, *Int. J. Quantum Chem.* **1996**, *57*, 281; (d) E. van Lenthe, J. G. Snijders, E. J. Baerends, *J. Chem. Phys.* **1996**, *105*, 6505; (e) E. van Lenthe, A. Ehlers, E.-J. Baerends, *J. Chem. Phys.* **1999**, *110*, 8943.
- [36] (a) A. D. Becke, *Phys. Rev. A* **1988**, *38*, 3098; (b) A. D. Becke, *J. Chem. Phys.* **1993**, *98*, 1372.
- [37] Y. Zhao, N. E. Schultz, D. G. Truhlar, *J. Chem. Phys.* **2005**, *123*, 161103.
- [38] Y. Zhao, D. Truhlar, *Theor. Chem. Acc.* **2008**, *120*, 215.
- [39] G. D. Purvis, III, R. J. Bartlett, *J. Chem. Phys.* **1982**, *76*, 1910.
- [40] T. H. Dunning, Jr., *J. Chem. Phys.* **1989**, *90*, 1007.
- [41] K. A. Peterson, D. Figgen, M. Dolg, H. Stoll, *J. Chem. Phys.* **2007**, *126*, 124101.
- [42] J. D. Watts, J. Gauss, R. J. Bartlett, *J. Chem. Phys.* **1993**, *98*, 8718.
- [43] F. Neese, E. F. Valeev, *J. Chem. Theory Comput.* **2010**, *7*, 33.
- [44] (a) K. Fukui, *Acc. Chem. Res.* **1981**, *14*, 363; (b) H. P. Hratchian, H. B. Schlegel, *J. Chem. Phys.* **2004**, *120*, 9918; (c) H. P. Hratchian, H. B. Schlegel, *J. Chem. Theory Comput.* **2004**, *1*, 61.
- [45] (a) G. te Velde, F. M. Bickelhaupt, E. J. Baerends, C. Fonseca Guerra, S. J. A. van Gisbergen, J. G. Snijders, T. Ziegler, *J. Comput. Chem.* **2001**, *22*, 931; (b) C. Fonseca Guerra, J. G. Snijders, G. te Velde, E. J. Baerends, *Theor. Chem. Acc.* **1998**, *99*, 391; (c) ADF2010.02, SCM, Theoretical Chemistry, Vrije Universiteit, Amsterdam, The Netherlands, available at: <http://www.scm.com> (accessed on 26 January 2012).
- [46] M. J. Frisch, G. W. Trucks, H. B. Schlegel, G. E. Scuseria, M. A. Robb, J. R. Cheeseman, G. Scalmani, V. Barone, B. Mennucci, G. A. Petersson, H. Nakatsuji, M. Caricato, X. Li, H. P. Hratchian, A. F. Izmaylov, J. Bloino, G. Zheng, J. L. Sonnenberg, M. Hada, M. Ehara, K. Toyota, R. Fukuda, J. Hasegawa, M. Ishida, T. Nakajima, Y. Honda, O. Kitao, H. Nakai, T. Vreven, J. A. Montgomery, Jr., J. E. Peralta, F. Ogliaro, M. Bearpark, J. J. Heyd, E. Brothers, K. N. Kudin, V. N. Staroverov, R. Kobayashi, J. Normand, K. Raghavachari, A. Rendell, J. C. Burant, S. S. Iyengar, J. Tomasi, M. Cossi, N. Rega, J. M. Millam, M. Klene, J. E. Knox, J. B. Cross, V. Bakken, C. Adamo, J. Jaramillo, R. Gomperts, R. E. Stratmann, O. Yazyev, A. J. Austin, R. Cammi, C. Pomelli, J. W. Ochterski, R. L. Martin, K. Morokuma, V. G. Zakrzewski, G. A. Voth, P. Salvador, J. J. Dannenberg, S. Dapprich, A. D. Daniels, Ö. Farkas, J. B. Foresman, J. V. Ortiz, J. Cioslowski, D. J. Fox, Gaussian 09, Revision C.01; Gaussian, Inc.: Wallingford CT, **2010**.
- [47] A. E. Reed, L. A. Curtiss, F. Weinhold, *Chem. Rev.* **1988**, *88*, 899.
- [48] (a) D. Feller, *J. Comput. Chem.* **1996**, *17*, 1571; (b) K. L. Schuchardt, B. T. Didier, T. Elsethagen, L. Sun, V. Gurumoorthi, J. Chase, J. Li, T. L. Windus, *J. Chem. Inf. Model.* **2007**, *47*, 1045.
- [49] M. Kohout, DGrid, version 4.6, Radebeul, 2011.
- [50] J. Contreras-García, M. Marqués, B. Silvi, J. Recio, In *Modern Charge-Density Analysis*; C. Gatti, P. Macchi, Eds.; Springer, New York, **2012**; pp. 625–658.
- [51] (a) I. Bytheway, R. J. Gillespie, T. -H. Tang, R. F. W. Bader, *Inorg. Chem.* **1995**, *34*, 2407; (b) R. J. Gillespie, I. Bytheway, T. -H. Tang, R. F. W. Bader, *Inorg. Chem.* **1996**, *35*, 3954.
- [52] R. J. Gillespie, S. Noury, J. Pilmé, B. Silvi, *Inorg. Chem.* **2004**, *43*, 3248.
- [53] W. Scherer, V. Herz, C. Hauf, In *Electron Density and Chemical Bonding*; D. Stalke, Ed.; Springer, Berlin, **2012**; pp. 159–207.
- [54] J.-F. Boily, T. M. Seward, *Geochim. Cosmochim. Acta* **2005**, *69*, 3773.
- [55] S. Moncho, G. Ujaque, P. Espinet, F. Maseras, A. Lledós, *Theor. Chem. Acc.* **2009**, *123*, 75.
- [56] R. B. Gomes, F. Illas, B. Silvi, *Chem. Phys. Lett.* **2004**, *388*, 132.
- [57] S. Raub, G. Jansen, *Theor. Chem. Acc.* **2001**, *106*, 223.
- [58] I. Vidal, S. Melchor, J. A. Dobado, *J. Phys. Chem. A* **2005**, *109*, 7500.
- [59] E. Matito, J. Poater, F. M. Bickelhaupt, M. Solà, *J. Phys. Chem. B* **2006**, *110*, 7189.
- [60] A. Martín Pendás, E. Francisco, M. A. Blanco, *Chem. Phys. Lett.* **2008**, *454*, 396.
- [61] F. Krausz, M. Ivanov, *Rev. Mod. Phys.* **2009**, *81*, 163.
- [62] A. H. Zewail, *Science* **2010**, *328*, 187.

Received: 5 April 2013
Revised: 8 May 2013
Accepted: 10 May 2013
Published online on 7 June 2013